

The fate of shear-oscillated amorphous solids

Cite as: J. Chem. Phys. **156**, 104902 (2022); <https://doi.org/10.1063/5.0079460>

Submitted: 21 November 2021 • Accepted: 07 February 2022 • Accepted Manuscript Online: 08 February 2022 • Published Online: 11 March 2022

 Chen Liu,  Ezequiel E. Ferrero, Eduardo A. Jagla, et al.



View Online



Export Citation



CrossMark

ARTICLES YOU MAY BE INTERESTED IN

[Microscopic structural origin behind slowing down of colloidal phase separation approaching gelation](#)

The Journal of Chemical Physics **156**, 084904 (2022); <https://doi.org/10.1063/5.0080403>

[Coupled cluster downfolding methods: The effect of double commutator terms on the accuracy of ground-state energies](#)

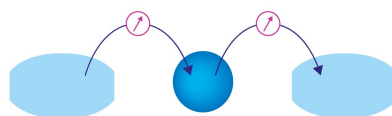
The Journal of Chemical Physics **156**, 094106 (2022); <https://doi.org/10.1063/5.0076260>

[Real-space density kernel method for Kohn–Sham density functional theory calculations at high temperature](#)

The Journal of Chemical Physics **156**, 094105 (2022); <https://doi.org/10.1063/5.0082523>

Webinar

Interfaces: how they make
or break a nanodevice



March 29th – Register now

 Zurich
Instruments



The fate of shear-oscillated amorphous solids

Cite as: J. Chem. Phys. 156, 104902 (2022); doi: 10.1063/5.0079460

Submitted: 21 November 2021 • Accepted: 7 February 2022 •

Published Online: 11 March 2022



View Online



Export Citation



CrossMark

Chen Liu,^{1,a)}  Ezequiel E. Ferrero,^{2,a)}  Eduardo A. Jagla,³ Kirsten Martens,⁴ Alberto Rosso,⁵
and Laurent Talon⁶

AFFILIATIONS

¹Laboratoire de Physique de l'Ecole Normale Supérieure, Paris, France

²Instituto de Nanociencia y Nanotecnología, CNEA-CONICET, Centro Atómico Bariloche, R8402AGP S. C. de Bariloche, Río Negro, Argentina

³Centro Atómico Bariloche, Instituto Balseiro, CNEA, CONICET, UNCUYO, R8402AGP S. C. de Bariloche, Río Negro, Argentina

⁴University Grenoble Alpes, CNRS, LIPhy, 38000 Grenoble, France

⁵Université Paris-Saclay, LPTMS, CNRS, 91405 Orsay, France

⁶Université Paris-Saclay, FAST, CNRS, 91405 Orsay, France

Note: This paper is part of the JCP Special Topic on Memory Formation.

^{a)} **Authors to whom correspondence should be addressed:** cl4175@columbia.edu and ferrero@cab.cnea.gov.ar

ABSTRACT

The behavior of shear-oscillated amorphous materials is studied using a coarse-grained model. Samples are prepared at different degrees of annealing and then subjected to athermal and quasi-static oscillatory deformations at various fixed amplitudes. The steady-state reached after several oscillations is fully determined by the initial preparation and the oscillation amplitude, as seen from stroboscopic stress and energy measurements. Under small oscillations, poorly annealed materials display *shear-annealing*, while ultra-stabilized materials are insensitive to them. Yet, beyond a critical oscillation amplitude, both kinds of materials display a *discontinuous* transition to the same *mixed* state composed of a fluid shear-band embedded in a marginal solid. Quantitative relations between uniform shear and the steady-state reached with this protocol are established. The transient regime characterizing the growth and the motion of the shear band is also studied.

Published under an exclusive license by AIP Publishing. <https://doi.org/10.1063/5.0079460>

I. INTRODUCTION

Amorphous solids are a vast class of materials, common in nature and ubiquitous for human applications. Their mechanical behavior is strongly affected by the preparation protocol: poorly annealed materials, such as emulsions, foams, or gels, are soft and ductile, while well annealed materials, such as metallic glasses, ceramics, and silica, are hard and brittle.^{1,2} Under a uniform deformation, the former tend to melt into a liquid, while the latter fail with a sharp stress-drop and the appearance of a thin liquid shear-band.^{3–6} Although we tend to distinguish between these two kinds of yielding, a debate is open: ductile materials could also display stress overshoots.^{6–9} Beyond finite-size issues,^{7–9} dealing only with transient states does not help to settle the discussion. This is where an oscillatory deformation protocol^{10–19} becomes handy, since it opens the possibility of characterizing a transition in terms of

stationary states. In molecular dynamics (MD) simulations, two different “phases” have been identified: For moderate strain amplitudes Γ , the material appears solid and is progressively annealed^{11,12,16–18} as oscillation cycles accumulate. Above a critical amplitude Γ_c , further shear-annealing is prevented and a shear-band coexists with a solid.^{11,12,17,18,20} Despite a rapidly growing literature,^{10–28,43} basic questions remain to be addressed: (i) the nature of the transition at Γ_c , (ii) the relation between steady-states in the two protocols (oscillatory and uniform shear), and (iii) how those states are reached.

To answer these questions, in this paper, we use a coarse-grained approach, which goes beyond natural limitations of MD simulations. We find that the transition from solid to flow at Γ_c is discontinuous. We quantitatively relate properties of the emerging phases in oscillatory shear with those of the uniform-deformation protocol. Moreover, we describe transient stages that are previously unexplored.

To do that, we prepare samples at different degrees of annealing, characterized by the initial energy E_{init} per unit volume, and subject them to oscillatory deformations at various fixed amplitudes Γ until steady-states are reached. We find that once a *driving condition* (E_{init}, Γ) is chosen, it univocally defines the material's fate in the steady-state, allowing us to fill a sort of *phase diagram*. Very well-annealed samples ($E_{\text{init}} < E^*$, with E^* being a critical annealing level) are insensitive to small oscillations, while poorly annealed samples ($E_{\text{init}} > E^*$) exhibit *shear-annealing* for a large enough sub-critical Γ . We, therefore, distinguish between *stable solids* that keep memory of their initial condition and *marginal solids* that result from the poorly annealed samples losing memory of their initial conditions due to the shear-annealing by oscillations. Yet, when the oscillation amplitude reaches the critical threshold $\Gamma_c(E_{\text{init}})$, every sample undergoes a *discontinuous transition*, comprising a jump in stress and energy, toward *the same* mixed solid–fluid state. Part of the system melts in a shear-band, while the rest becomes a critical solid of energy E^* , independently of the initial condition. The fluid in the band corresponds to one of the stationary states at a large uniform quasi-static shear and holds, at most, the uniform yield stress Σ_y . As Γ is further increased, the width of the shear-band scales as a power of $(\Gamma - \Sigma_y/\mathcal{S})$, with \mathcal{S} being the effective shear-modulus, further relating uniform and oscillatory protocols. In addition, a rich transient dynamics toward the steady-state above Γ_c is unveiled. We show a bandwidth growth as a function of the number of oscillation cycles that is reminiscent of critical domain coarsening. Surprisingly, once the band reaches its stable width, it ballistically sweeps out the deeply annealed regions, if present, turning them into the critical solid of energy E^* , and finally displays an (anomalous) diffusion. Overall, our paper offers answers to fresh issues raised by MD simulations of glasses.

II. METHOD

Our modeling is based on the evolution of a two-dimensional scalar strain field in a disordered potential, previously used to study yielding under uniform deformation.^{29–33} Initial sample annealing is achieved by tuning the configuration of the disordered landscape (lower initial energies E_{init} for better annealed systems). Within this picture, the strain field behaves as a manifold propagating in a disorder medium.^{30,31,34} Two essential ingredients are incorporated: the quadruple Eshelby's elastic interaction^{2,35} and a disorder that rather than originating in quenched impurities mimics the random positions of particles. The local disorder changes irreversibly, even if the strain manifold revisits the same location. Details of our method are presented in [Appendix A](#).

III. RESULTS

In view of their relevance in interpreting the shear oscillation results, we first reproduce some key features in uniform shear. In [Fig. 1\(a\)](#), we show stress–strain curves for individual samples prepared at different degrees of annealing E_{init} (see also [Appendix B](#)). After an initial linear elastic response of slope $\mathcal{S} \approx 0.91$, all samples at large strain $\gamma \gtrsim 3$ reach a common plateau corresponding to the yield stress $\Sigma_y = 0.375 \pm 0.003$. The characteristic strain γ_y , where plasticity becomes important, is estimated as $\gamma_y = \Sigma_y/\mathcal{S} \approx 0.413$. Poorly annealed materials display a monotonic crossover from an

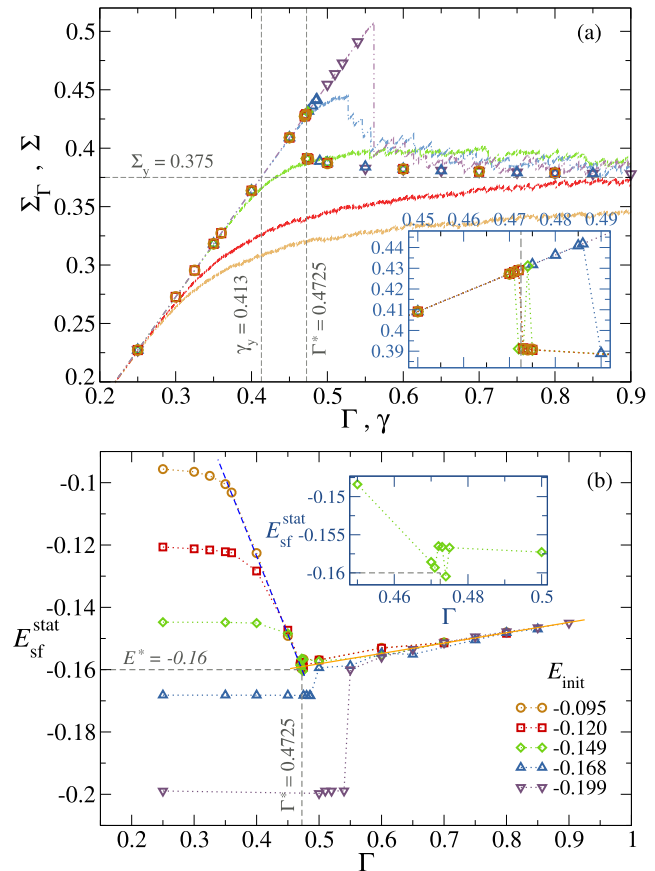


FIG. 1. Stationary properties. (a) Symbols—Maximum stress Σ_T vs the oscillatory strain amplitude Γ . Curves—Stress–strain (Σ vs γ) produced by the quasi-static uniform shear. Different colors code for different degrees of initial annealing signaled in the bottom panel. The inset shows a zoomed-in view of the transition region. The system size is 128^2 . (b) Stress-free steady energy $E_{\text{sf}}^{\text{stat}}$ vs Γ . The purple dashed-line corresponds to “marginal solids.” The orange solid line displays a fit of $E_{\text{sf}}^{\text{stat}}(\Gamma)$ discussed in the text. The inset shows a zoomed-in view of the transition region (only $E_{\text{init}} = -0.149$ is shown).

elastic solid to a liquid crossing γ_y , while well annealed systems remain elastic above γ_y up to a failure strain γ_f where a sharp stress downfall occurs. The overshoot gets larger for better annealed samples.^{4–6,9} In general, the total energy per volume of the material can be decomposed into two contributions: $E_{\text{tot}} = E_{\text{sf}} + \Sigma^2/(4\mu)$, where the second contribution is due to macroscopic elastic deformation (with $\mu = 1/2$ being the shear modulus), and E_{sf} , called the “stress-free energy” afterward, characterizes the state of the material with zero macroscopic stress. In the large uniform shear limit $\gamma \rightarrow \infty$, where the memory of the initial state is completely erased, all samples converge to a homogeneous stationary liquid state with $E_{\text{sf}}^{\text{stat}} = -0.122 \pm 0.001 \equiv E_{\text{liq}}$ (see [Fig. 7](#)).

A. Steady-state properties

Now, in our oscillatory protocol, the material is deformed by quasi-statically varying the strain from 0 to Γ , then to $-\Gamma$, and

subsequently back to 0 to complete one cycle of amplitude Γ . This cycle is repeated until a steady-state is reached. By varying Γ and E_{init} , we obtain an assortment of stationary states. Figure 1(a) shows the steady-state maximum stress^{11,16,20} $\Sigma(\Gamma) = \frac{1}{2}(\Sigma(-\Gamma) + \Sigma(+\Gamma))$ as a function of Γ in comparison with uniform-shear load curves. The symmetric definition of Σ_Γ is motivated in the need of suppressing the bias caused by the abundant plasticity in the initial direction of the shear. Consistent with the MD results, all samples exhibit a sharp jump of $\Sigma(\Gamma)$ at a critical strain amplitude $\Gamma_c(E_{\text{init}})$. The moderately annealed samples ($E_{\text{init}} = -0.095, -0.12$, and -0.149) fail at the same $\Gamma_c \approx 0.4725 \equiv \Gamma^*$, independently of the initial degree of annealing, while the more annealed samples ($E_{\text{init}} = -0.168$ and -0.199) experience a later and stronger failure at $\Gamma_c(E_{\text{init}}) \approx \gamma_f(E_{\text{init}}) > \Gamma^*$, as better annealed is the sample. Once above Γ_c , the steady-state stress Σ_Γ for any initial state is well identified with Σ_γ of a stationary flowing state in the quasi-static uniform shear deformation. Figure 1(b) displays the stationary stress-free energy $E_{\text{sf}}^{\text{stat}}$ as a function of Γ . Here, using the stress-free energy E_{sf} has the advantage to characterize the intrinsic state without the external load, while the stroboscopic energy^{11,27,28} incorporates an arbitrary elastic contribution when $\Gamma > \Gamma_c$. For a very small Γ , the stationary state $E_{\text{sf}}^{\text{stat}}$ strongly depends on E_{init} . By increasing Γ within the solid phase ($\Gamma < \Gamma_c$), two scenarios separated by a critical annealing $E^* \approx -0.16$ are observed. Samples with $E_{\text{init}} < E^*$ keep a perfect memory of their initial states up to melting, evidenced by $E_{\text{sf}}^{\text{stat}}(\Gamma) = E_{\text{init}}$ for all $\Gamma < \Gamma_c(E_{\text{init}})$.^{16,26} Yet, for $E_{\text{init}} > E^*$, the phenomenology is richer: By increasing Γ , at some point, the stationary-state $E_{\text{sf}}^{\text{stat}}$ starts to decrease with the amplitude, losing memory of the initial condition. This is a manifestation of shear-annealing in the steady-state, as similarly observed in Refs. 11, 16, and 26–28. Note that for initially weakly annealed systems, there exists also a *transient* process of shear-annealing (described later on), where samples reach a lower-energy steady-state by oscillating at a fixed Γ . $E_{\text{sf}}^{\text{stat}}$ for $E_{\text{init}} > E^*$ ends up collapsing to a common curve [purple dashed line in Fig. 1(b)], where the initial condition becomes irrelevant and $E_{\text{sf}}^{\text{stat}}$ depends only on Γ . We call “marginal solids” as the stationary states lying on the purple dashed line, which terminates at Γ^* at the critical energy E^* . Once $\Gamma > \Gamma_c(E_{\text{init}})$, both Σ_Γ and $E_{\text{sf}}^{\text{stat}}(\Gamma)$ fall onto a unique curve, independent of E_{init} . The system develops a permanent liquid shear-band embedded in a solid phase, and the steady-state energy $E_{\text{sf}}^{\text{stat}}$ increases with Γ [Fig. 1(b)] (see also Refs. 16, 20, and 27). From the previous discussion, we can associate to each E_{init} an amplitude $\Gamma_a(E_{\text{init}})$ above which the steady-state $E_{\text{sf}}^{\text{stat}}(\Gamma, E_{\text{init}})$ is independent of the initial annealing E_{init} .

As summarized in a diagram in Fig. 2, $\Gamma_a(E_{\text{init}})$ (dashed line) identifies with $\Gamma_c(E_{\text{init}})$ (solid line) below E^* and bifurcates above it. The solid steady-states resulting from driving conditions below $\Gamma_a(E_{\text{init}})$ are strongly reminiscent of the initial state and called “stable solids.” In contrast, those driving conditions in between Γ_c and Γ_a correspond to solids that forget their initial condition and end up being “marginal solids” in the steady-state. Driving conditions in the region above $\Gamma_c(E_{\text{init}})$ lead to a steady-state mixed phase composed of a fluid shear band surrounded by a critical marginal solid, which we detail in the following.

Figure 3 shows the averaged stress-free energy profile across a section orthogonal to the shear-band³⁶ (evidenced in the strain field in the left-inset). The energy profile characterizes the band

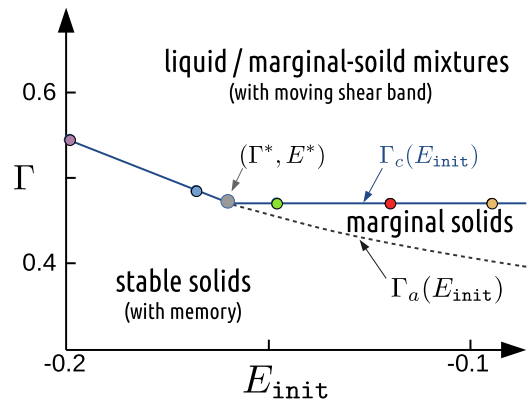


FIG. 2. “Phase diagram” classifying driving conditions (E_{init}, Γ) according to the steady-state they will reach: *stable solids* (strongly reminiscent of the initial state), *marginal solids* (shear-annealed solids independent of the initial condition), and *solid–liquid mixtures* characterized by an erratic shear-band. Colored circles indicate Γ_c for different initial degrees of annealing E_{init} .

as a bell-shape. The interior of the band (top of the bell) has the same energy as the stationary liquid in uniform shear deformation $E_{\text{liq}} \approx -0.122$. The width w_s of the band increases with Γ and is well fitted by $w_s(\Gamma) = a(\Gamma - \Gamma_0)^\alpha$. A good collapse is found when rescaling the profiles with $\alpha = 1/2$ (right-inset of Fig. 3), reminiscent of the transient band dynamics in uniform shear.³⁷ We further notice two peculiarities: First, from the fit, Γ_0 identifies with γ_y , instead of Γ^* , implying that at the transition, the shear-band has a finite width $w_s(\Gamma^*) > 0$ (because $\gamma_y < \Gamma^*$). Second, the energy profile is independent of E_{init} and the energy at the bottom of the bell-shape coincides with the critical solid energy E^* . This allows us to conclude that the mixture phase is completely independent of the initial degree of annealing and uniquely characterized by the width w_s : the stationary regime is composed of a fraction of critical solid at energy E^* and a shear-band made of the liquid of energy E_{liq} . Since $E_{\text{liq}} > E^*$,

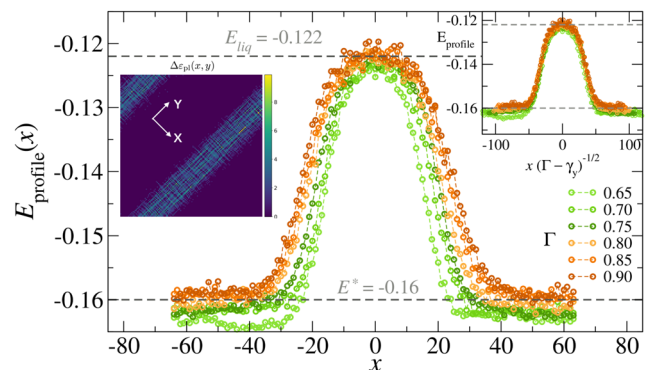


FIG. 3. Energy profiles averaged along the y axis for different Γ . $x = 0$ is set to the maximum location. (Left inset) Map of strain field during a half-cycle in the steady-state. (Right inset) Profiles collapse using $w_s(\Gamma) = a(\Gamma - \Gamma_0)^\alpha$ with $\Gamma_0 = \gamma_y = 0.413$ and $\alpha = 1/2$.

monotonic growth of E_{sf}^{stat} [Fig. 1(b)] can be rationalized in terms of the shear-band widening with Γ ,

$$E_{sf}^{stat} \simeq E^* + (E_{liq} - E^*) \frac{a(\Gamma - \gamma_y)^\alpha}{L}. \quad (1)$$

The validity of this behavior is tested in Fig. 1(b) (orange line). From our analysis, the transition seems to be of first order in nature for two reasons: First, the jump in E_{sf}^{stat} is clearly discrete for well annealed samples, but it appears discontinuous also for the poorly annealed systems, where around Γ^* , we observe energy fluctuations between two close but distinct levels [see the inset of Fig. 1(b)]: $E_{sf}^{stat} \approx -0.16$ for the realizations that remain in the solid phase and $E_{sf}^{stat} \approx -0.157$ for those that transition to the mixed phase. Second, from the finite-size analysis of E_{sf}^{stat} showing a nice collapse of E_{sf}^{stat}

for different system sizes L in Fig. 9, we can conclude that the shear band when appearing invades a finite portion of the system $w_s(\Gamma^*)/L > 0$. The first-order nature of the transition in energy E_{sf}^{stat} at Γ^* is further elaborated in Appendix D.

B. Transient properties

We now discuss the transient oscillatory dynamics. Figure 4 shows the evolution of $E_{sf}(n)$, as the oscillation cycles n accumulate, for different driving conditions (E_{init}, Γ). Below Γ_c [Fig. 4(a)], ultra-stable systems ($E_{init} < E^*$) are unperturbed by the oscillations, while systems with $E_{init} > E^*$ shear-anneal if the amplitude is large enough. At amplitudes above $\Gamma_a(E_{init})$, all initial conditions are shear-annealed to the same stationary state, as observed for our three softest samples in Fig. 4(a). Above Γ_c [Fig. 4(b)], all samples go to the same stationary state at large n . Our observations for the number n_T of cycles to reach steady-states are compatible with a divergence when approaching Γ_c reported in previous works.^{11,14,15,17,20} Data for ($\Gamma < \Gamma_c$) are shown in Appendix E.

We switch now to the observation of different dynamical regimes for the mixed phase. For poorly annealed samples, the onset of the shear-band and its stabilization in a stationary width $w_s(\Gamma)$ occur gradually and rapidly as the solid region shear-anneals to the critical state in a small number of cycles. Then, the shear band diffuses in the material [see Fig. 5(a) and Video 1 (Multimedia view)] with a mobility that increases with Γ . In well annealed systems, instead, the transient is richer and we identify three dynamical regimes [Fig. 5(b), see also Video 2 (Multimedia view)]: (i) *Shear band formation and growth*. The initial band growth is observed at the top of Fig. 5(b) (see Fig. 11 in for a more detailed illustration for the initial band growth). This initial coarsening of the shear-band is studied in Fig. 6 at different Γ . In all cases, the bandwidth grows as $\sim n^{1/3}$ until reaching the stationary width $w_s \sim (\Gamma - \gamma_y)^{1/2}$. (ii) *Melting of the solid*. The now fully formed shear band displays a ballistic motion preferentially invading the deeply annealed solid and leaving behind the critical solid of energy E^* . (iii) *Shear band*

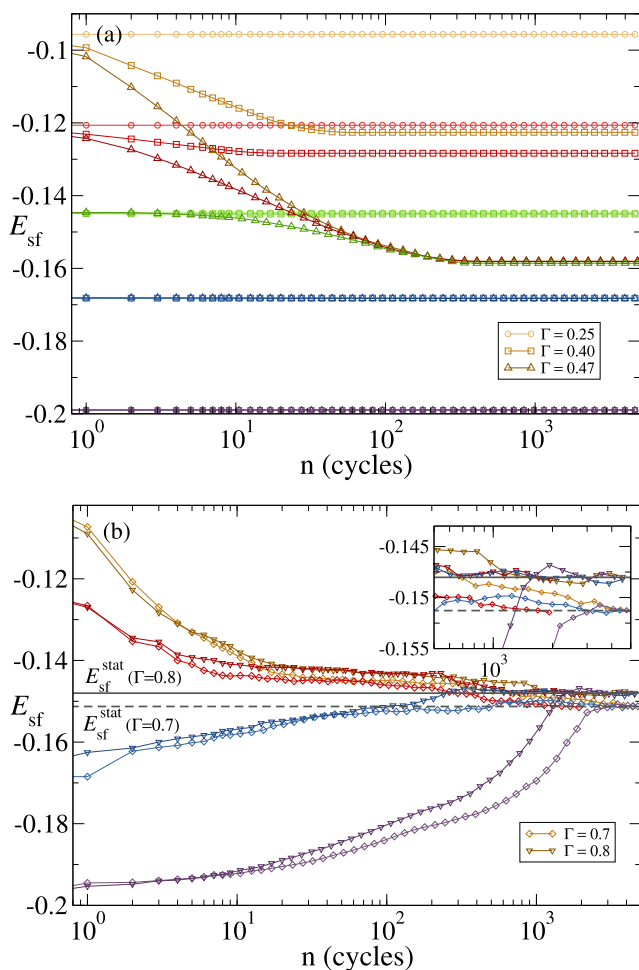


FIG. 4. Transient properties—Evolution of stress-free energy E_{sf} as the number of cycles n increase for different amplitudes. Color codes for different E_{init} are the same as in Fig. 1. The system size is 128^2 . (a) Solid phase ($\Gamma < \Gamma_c$) and (b) mixed phase ($\Gamma > \Gamma_c$). The inset shows a zoomed-in view to appreciate the difference in E_{sf}^{stat} at different Γ .

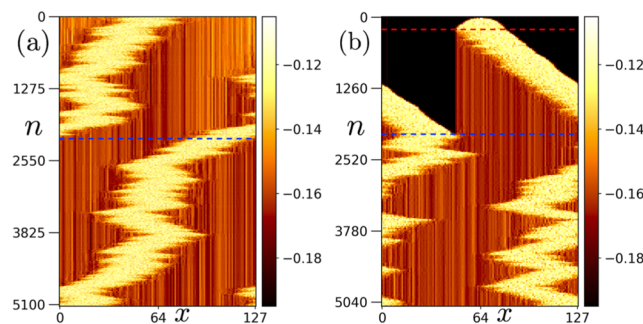


FIG. 5. Energy profiles $E_{profile}(x)$ evolving as a function of the number n of oscillation cycles for $\Gamma = 0.7$. Light colors represent higher energies and evidence the position of the shear-band. (a) A poorly annealed sample with $E_{init} \approx -0.12$ [see also Video 1 (Multimedia view)]. (b) A well annealed sample with $E_{init} \approx -0.199$ [see also Video 2 (Multimedia view)]. The red dashed-line in (b) indicates the stabilization of the bandwidth at $n \approx 220$. When the blue dashed-line is reached, the band has visited the entire system. Multimedia views: (a) <https://doi.org/10.1063/5.0079460.1>; (b) <https://doi.org/10.1063/5.0079460.2>

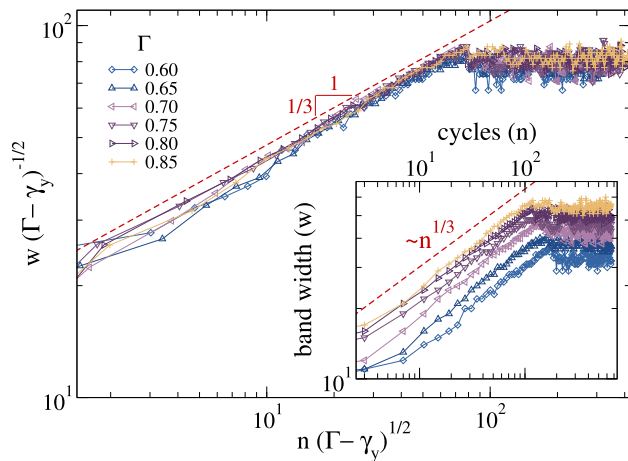


FIG. 6. Shear-bandwidth w as a function of n for different Γ . The initial condition is a well annealed solid ($E_{\text{init}} = -0.168$). The inset shows raw-data and the main panel shows the scaling $w(\Gamma - \gamma_y)^{-1/2}$ vs $n(\Gamma - \gamma_y)^{1/2}$. The red dashed line is a power-law $\sim n^{1/3}$. The system size is 256^2 .

diffusion. When the shear-band has visited the entire system, all the regions outside the band have been modified into the critical marginal solid. The stationary state is reached and the band diffuses forever, maintaining its characteristic Γ -dependent width.

IV. DISCUSSION

Our mesoscopic model allows us to recover the phenomenology of the oscillatory shear of amorphous materials reported by MD simulations^{4,11,16,26,28} and go beyond. While some emerging features can already be captured by even further simplified toy models as seen recently,¹⁴ keeping a spatial extent for the system and its geometry gives access to the full picture. We are able to univocally classify the oscillatory stationary states according to a “phase diagram” in the space of oscillation amplitude Γ and initial annealing level E_{init} and relate them with the steady-states of the uniform-deformation protocol. Interestingly, the oscillatory protocol always shows a discontinuous first order like Ref. 43, transition in both stress and energy at a critical strain amplitude Γ_c , even in the case of ductile materials that melt homogeneously under uniform deformation. Notably, ductile materials mechanically anneal and harden at sub-critical amplitudes under oscillatory shear. Independently of the initial state, every system sheared at large amplitudes ends up in a steady-state displaying a permanent shear-band. This band contains a stationary fluid identical to the one obtained at large uniform deformations and is embedded in a solid matrix, which is not at all arbitrary. The solid surrounding the shear-band in this mixed phase is the critical marginal solid that has the energy of the critical annealing level E^* . A line of *amnesia* $\Gamma_a(E_{\text{init}})$ discriminates driving conditions (E_{init}, Γ) between *stable solids* and solids that shear-anneal and evolve toward a marginal line in the steady-state. Our approach also gives transparent access to the transient regimes of shear-band formation, growth, and motion. For deeply annealed samples, a small but finite width band first spreads the system, then grows with a power-law $\propto n^{1/3}$ of the number of oscillation cycles. Ultimately, the band

invades ballistically the deeply annealed solid, leaving behind the critical solid of energy E^* . Finally, it diffuses anomalously over all the systems.

These results shed light to clarify some previous observations in the literature and open interesting directions of new research. One could ask, for example, whether the emergence of a transient state of multiple shear-bands is possible in the large system limit and how do they merge in a single band in the steady-state (or not). In addition, to which extent the incorporation of “reversible” plastic events observed in atomistic simulations^{17–21,24,25} enriches the overall phenomenology. Those are absent in our present model by choice but easy to include by locally quenching the disordered potential.¹⁵ Furthermore, the critical annealing E^* detected in the oscillatory protocol could also play a relevant role in the uniform shear, where the ductile–brittle yielding transition is a matter of vivid discussion.^{4,6,9} It is, indeed, suggestive that the load curve of our closest to E^* sample sits near to the apparent transition between ductile/brittle yielding probed by the uniform shear curves. More importantly, it will be interesting to test experimentally these predictions, with new measurements closer to the quasi-static limit, since in the standard setups, the oscillations are relatively fast and the material softens instead of annealing and hardening.

Moreover, general features of our phase diagram could find analogies in different systems with elastic interactions, irreversible events, and quenched disorder, such as vortex or skyrmion systems where the initial state can also be prepared in different ways.^{38–41} In general, we hope that our results will motivate new research directions in the study of low temperature amorphous materials, from realistic large-scale atomistic simulations to experiments.

ACKNOWLEDGMENTS

We are indebted to M. Ozawa for illuminating discussions on the subject. We thank S. Sastry for kind feedback on an earlier version of this paper. We acknowledge support from the collaboration project ECOS Sud-MINCYT A16E01 and the IRP project “Statistical Physics of Materials” funded by CNRS, C.L., A.R., and L.T. acknowledge support from “Investissement d’Avenir” LabEx PALM (Grant No. ANR-10-LABX-0039-PALM).

AUTHOR DECLARATIONS

Conflict of Interest

The authors have no conflicts to disclose.

DATA AVAILABILITY

The data that support the findings of this study are available from the corresponding authors upon reasonable request.

APPENDIX A: METHODS: OUR MODEL

We focus on two-dimensional systems. Our goal is to provide a description of the physics of amorphous materials under deformation and we use a model based on the evolution of the three strain field components:^{29,42} the isotropic compression $\varepsilon_1(\mathbf{r})$ and the shear components $\varepsilon_2(\mathbf{r})$ and $\varepsilon_3(\mathbf{r})$. The latter are bi-axial deformations (compression along some direction, expansion perpendicularly),

and the difference between $\varepsilon_2(\mathbf{r})$ and $\varepsilon_3(\mathbf{r})$ is that the compression/expansion axis are the $x - y$ axis for the first and the lines at 45° for the second [recall that given the continuum displacement field, $\mathbf{u}(\mathbf{r}) = (u_1(\mathbf{r}), u_2(\mathbf{r}))$, the elements of strain tensor are given by $\varepsilon_{ij}(\mathbf{r}) = \frac{1}{2}(\partial_i u_j(\mathbf{r}) + \partial_j u_i(\mathbf{r}))$. Then, $\varepsilon_1(\mathbf{r}) = (\varepsilon_{11}(\mathbf{r}) + \varepsilon_{22}(\mathbf{r}))/2$, $\varepsilon_2(\mathbf{r}) = (\varepsilon_{11}(\mathbf{r}) - \varepsilon_{22}(\mathbf{r}))/2$, and $\varepsilon_3(\mathbf{r}) = \varepsilon_{12}(\mathbf{r})$]. For a perfectly elastic solid, one can write the energy of any deformation in terms of a quadratic elastic functional

$$E_{\text{elast.}} = \int d^2\mathbf{r} (B\varepsilon_1^2 + \mu\varepsilon_2^2 + \mu\varepsilon_3^2), \quad (\text{A1})$$

where B and μ are, respectively, the bulk and shear moduli. Here, we use $B = 1$ and $\mu = 1/2$. This purely elastic functional has a single minimum, which corresponds to the undeformed state. When a deformation is applied, it brings the system out of such a minimum; when released, a restoring stress brings the system back to its undeformed state. If we want to take plasticity into account, irreversible deformations should be allowed; for example, the energy landscape may be characterized by multiple local minima separated by finite barriers (similar to the case of sheared vortices in random quenched potentials^{39,41}). Here, we study the response of the material under simple shear. We account for the plastic events by replacing the harmonic term $\mu\varepsilon_3^2$ in Eq. (A1) with a disordered potential $V_{\underline{x}}[\mathbf{r}, \varepsilon_3]$ that displays many minima as ε_3 varies. The other two strain components, ε_1 and ε_2 , are expected to remain small, and the quadratic approximation is expected to hold. The energy functional then becomes

$$E_{\text{plast.}} = \int d^2\mathbf{r} (B\varepsilon_1^2 + \mu\varepsilon_2^2 + V_{\underline{x}}[\mathbf{r}, \varepsilon_3]). \quad (\text{A2})$$

The subscript of $V_{\underline{x}}$ represents an internal degree of freedom. Thus, the disorder potential is not a function of the strain field $\varepsilon_3(\mathbf{r})$ only. The origin of that internal degree of freedom is justified as follows: In amorphous materials, the disorder is not generated by immobile impurities but rather by the random-like configurations of the particle position \underline{x} . Plastic events, called *shear transformations*, are localized in space. When an event occurs in the region \mathbf{r} , the particles inside the region rearrange irreversibly from \underline{x} to \underline{x}' . This rearrangement is mimicked in the model by two features.

- First, $\varepsilon_3(\mathbf{r})$ overcomes a local energetic barrier and reaches the basin of a new minimum of the disordered potential.
- Second, the basin of the old minimum also modifies irreversibly as new configuration of particle positions imposes a new disorder potential.

In the spirit of keeping only the essence of the physical process involving local plastic events, we model the disorder of each region \mathbf{r} as a collection of pieces of harmonic potential,

$$V_{\text{parab}}(\varepsilon_3) = \mu[(\varepsilon_3 - \varepsilon_{pl})^2 - \varepsilon_w^2] \quad \text{for } |\varepsilon_3 - \varepsilon_{pl}| < \varepsilon_w. \quad (\text{A3})$$

The random parameters ε_{pl} and ε_w vary from region to region: ε_{pl} defines the location of the minimum and ε_w defines the semi-width of the potential. Once the strain ε_3 overcomes the barriers of the parabolic basin, a new semi-width ε_w' is drawn from a triangular distribution of mean $1/2$ and standard-deviation $1/20$. The new minimum of the potential is updated as follows:

- When ε_3 overcomes the barrier at $\varepsilon_{pl} - \varepsilon_w$, the new minimum is located at $\varepsilon_{pl} - (\varepsilon_w + \varepsilon_w')$.
- When ε_3 overcomes the barrier at $\varepsilon_{pl} + \varepsilon_w$, the new minimum is located at $\varepsilon_{pl} + (\varepsilon_w + \varepsilon_w')$.

It is important to stress that once strain ε_3 overcomes the barriers of the parabolic basin, the local basin changes irreversibly, even if ε_3 moves backward.

The three components of the strain field are not independent but obey the St. Venant constraint.²⁹ As a consequence, the deformation of the material can be described by the evolution of a single component. In particular, assuming, in the framework of an overdamped dynamics, that ε_1 and ε_2 relax much faster than ε_3 , we arrive at

$$\partial_t \varepsilon(\mathbf{r}, t) = \int d^2\mathbf{r}' G(\mathbf{r} - \mathbf{r}') \varepsilon(\mathbf{r}') + \eta_{\underline{x}}(\mathbf{r}, \varepsilon) + \Sigma_{\text{ext}}. \quad (\text{A4})$$

Here, $\varepsilon(\mathbf{r}, t)$ has replaced $\varepsilon_3(\mathbf{r}, t)$ for a lighter notation and the kernel $G(\mathbf{r})$ is the long-range Eshelby's propagator. For simple shear, using the method in Ref. 42, the propagator can be written in terms of the polar coordinates $\mathbf{r} = (r, \theta_r)$ as

$$G(\mathbf{r}) = \frac{2\sqrt{2}B}{\pi r^2} \frac{3 \cos(4\theta_r) - 1}{(3 - \cos(4\theta_r))^2}. \quad (\text{A5})$$

Finally, $\eta_{\underline{x}}$ is originated from the disorder potential as $-\partial_{\varepsilon} V_{\underline{x}}$ and Σ_{ext} is the external applied stress.

For our purposes, it is important to control the macroscopic strain instead of the macroscopic stress. In order to achieve this, one can replace Σ_{ext} with $\kappa(\gamma - \bar{\varepsilon})$ in Eq. (A4) [$\bar{\varepsilon}$ indicates the macroscopic strain defined as the spatial average of $\varepsilon(\mathbf{r})$]. For large values of κ , it is expected that the macroscopic strain $\bar{\varepsilon}$ is close to γ . The slope of the stress-strain curve is given by $\mathcal{S} = 2\kappa\mu/(\kappa + 2\mu)$. Here, we use $\kappa = 10$ and $\mu = 1/2$, so we get $10/11 \approx 0.91$ used as the initial slope of the stress-strain curve in the main text.

The energy functional defined in Eq. (A2) can be equivalently written as

$$E_{\text{plast.}}[\varepsilon(\mathbf{r})] = \int d^2\mathbf{r} e(\mathbf{r})$$

with

$$e(\mathbf{r}) \triangleq \frac{1}{2} \varepsilon(\mathbf{r}) \int d^2\mathbf{r}' G(\mathbf{r} - \mathbf{r}') \varepsilon(\mathbf{r}') + V_{\underline{x}}(\mathbf{r}, \varepsilon(\mathbf{r})). \quad (\text{A6})$$

Thus, our system can be viewed as an elastic manifold $\varepsilon(\mathbf{r})$ (with long-range interactions among all sites) living in an energy landscape where each site has its independent disordered potential. The stress-free energy used in the main text is then defined as the plastic energy per site: $E_{\text{st}} \triangleq E_{\text{plast.}}[\varepsilon^*]/L^2$ with $\left. \frac{\delta E_{\text{plast.}}}{\delta \varepsilon(\mathbf{r})} \right|_{\varepsilon^*} = 0$. The energy profiles of the main text are obtained by averaging the local energy to $e(\mathbf{r})$ along the direction of the shear band. We apply quasi-static deformation γ by numerically solving Eq. (A4) mapped onto a lattice system.

Special care is taken for the initial condition, since we want to mimic different degrees of annealing in our samples. In our model, a well-annealed sample corresponds to an initial condition where the local strains are confined in deep potential wells, while poorly annealed samples correspond to a strain manifold confined in shallow potential wells. In practice, we start from a liquid configuration of local energy basins obtained after a long uniform shear. Then, to prepare samples of different degrees of annealing, we change the depths of the parabolic wells, ε_w . To obtain deeply annealed

samples, we also align the centers, ε_{pl} , to their mean value. Finally, we let the local strain relax to its stress-free configuration and that makes our initial condition to start the oscillatory deformation. We performed simulations for systems of sizes $N = 32 \times 32, 64 \times 64, 128 \times 128, 256 \times 256$. The data shown in this work correspond to the two largest systems.

APPENDIX B: UNIFORM SHEAR DEFORMATION CURVES

We present in this section more detailed results for the case of uniform shear deformation. In Fig. 7(a), we show the same stress-strain curves as Fig. 1(a) of the main text with a larger scope of strain up to $\gamma = 4$ so that the common plateau $\Sigma_y \approx 0.375 (\pm 0.003)$ at long strains is well captured. We show system's stress-free energy

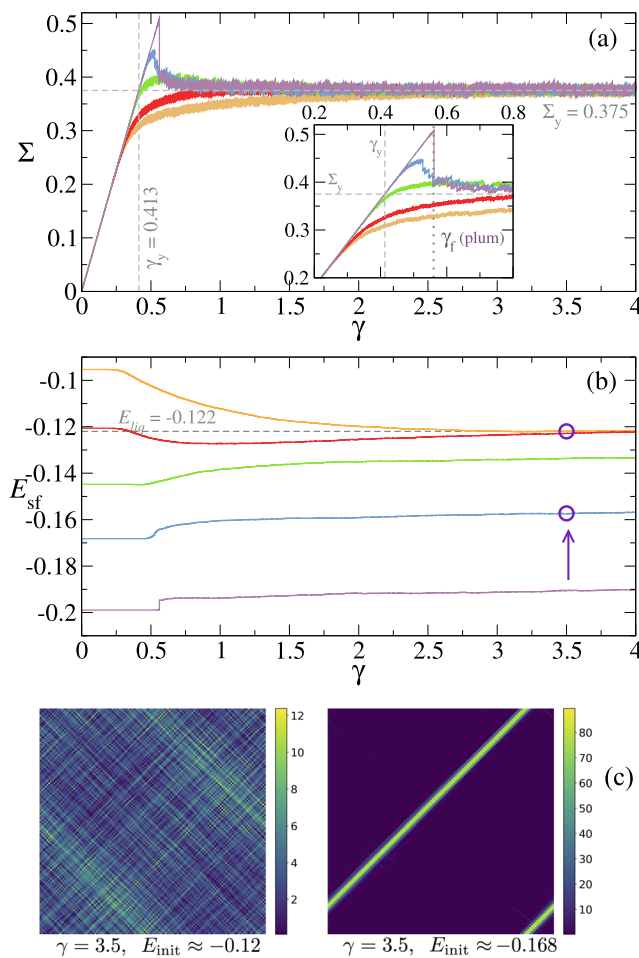


FIG. 7. Uniform shear deformation for different degrees of initial annealing [$E_{init} \approx -0.095$ (chocolate), -0.12 (red), -0.149 (chameleon), -0.168 (blue), and -0.199 (plum)]. (a) Stress-strain curves for different initial degrees of annealing. The yield stress $\Sigma_y = 0.375$ defined as the plateau is also indicated. (b) Evolution of the stress-free energy $E_{sf} = E(\Sigma) - \Sigma^2/(4\mu)$ during the deformation. The stationary plateau $E_{liq} = -0.122$ is also indicated. (c): Color map of the local deformation field at $\gamma = 3.5$ for two samples prepared at different degrees of annealing, circles in (b).

as a function of strain in Fig. 7(b). Poorly annealed samples (those which do not display a failure) reach rather quickly a common energy plateau $E_{liq} \approx -0.122 (\pm 0.001)$, which corresponds to the fully formed stationary liquid state. In contrast, well annealed samples display different and slowly evolving transient regimes. These differences can be understood as follows: Poorly annealed systems melt at deformations around γ_y into a non-Newtonian liquid, which has no memory of the initial degree of annealing (see Fig. 7 bottom left). In well annealed systems, instead, the non-Newtonian liquid is localized within a shear band and the solid part is unchanged, insensitive to the deformation (see Fig. 7 bottom right). When γ is increased further, the band widens. As discussed in Ref. 37, we expect $w(\gamma) \propto \sqrt{\gamma - \gamma_f}$. Eventually, for a very large γ , the bandwidth reaches the system size and the whole sample lose memory of the initial condition converging to the stationary value E_{liq} .

APPENDIX C: TYPICAL LOOPS IN OSCILLATORY STATIONARY STATES

In Fig. 8, we show the total energy E (per volume) as a function of γ during a steady oscillation between $\pm\Gamma$. In the solid phase

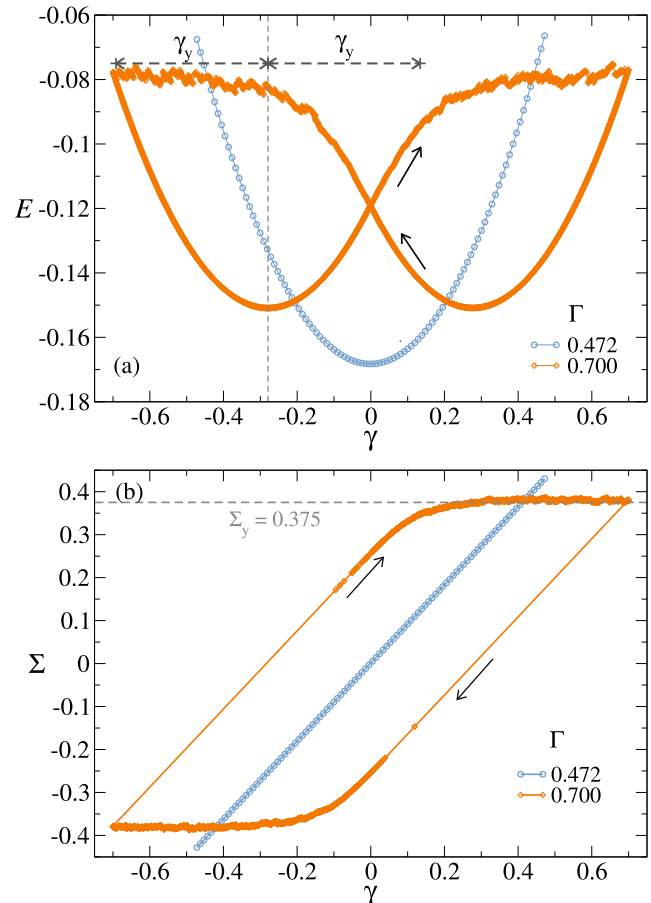


FIG. 8. (a) Energy vs strain in the oscillatory steady state (only one loop shown) for $\Gamma = 0.45$ (light-blue circles) and $\Gamma = 0.7$ (orange diamonds). The little black arrows mark the sense of the loop. (b) Stress as a function of strain in the oscillatory steady state for the same two amplitudes as above.

($\Gamma < \Gamma_c$), the energy displays a single parabolic shape, corresponding to an elastic behavior, while in the mixed phase ($\Gamma > \Gamma_c$), the energy has a butterfly shape: two shifted parabolas are followed by a noisy plateau that reveals the presence of the liquid state. The two parabolas have an extension of γ_y at both sides and the maximal stress, at $\pm\Gamma$, saturates to Σ_y , which also supports that the shear band is made of the stationary liquid state at large uniform shear, where plasticity dominates the dynamics once sheared beyond γ_y from a zero stress state.

APPENDIX D: THE DISCONTINUOUS TRANSITION IN E_{sf}^{stat} ACROSS Γ^*

In Fig. 9, we observe that at different amplitudes Γ , E_{sf}^{stat} (namely, the steady-state stress-free energies per unit volume) does not depend on the system size. As a consequence, in the mixed phase, for $\Gamma > \Gamma_c \geq \Gamma^*$, the shear band invades a finite fraction $r = w_s/L$ of the system, with w_s representing the width of the shear band. We can evaluate this fraction by observing that in the stationary state, during the oscillation driving from $-\Gamma$ to Γ , the material behaves initially as a solid and accumulates an elastic strain $\approx 2\gamma_y$ (see, e.g., Fig. 8), and the rest of the macroscopic deformation $2\Gamma - 2\gamma_y$ consists of the plasticity confined within the shear band, denoted by γ_{plt} . Formally, one may write

$$2\Gamma - 2\gamma_y = r\gamma_{plt}. \quad (D1)$$

Since plasticity takes place significantly only during the loading from $-\Gamma + 2\gamma_y$ to $+\Gamma$, it is reasonable to assume

$$\gamma_{plt} \propto (2\Gamma - 2\gamma_y)^x \quad \text{with } x > 0. \quad (D2)$$

Combining the two relations results in

$$\begin{aligned} r(\Gamma) &= K(\Gamma - \gamma_y)^{1-x}, \\ w_s(\Gamma) &= r \cdot L = a(\Gamma - \gamma_y)^{1-x}, \end{aligned} \quad (D3)$$

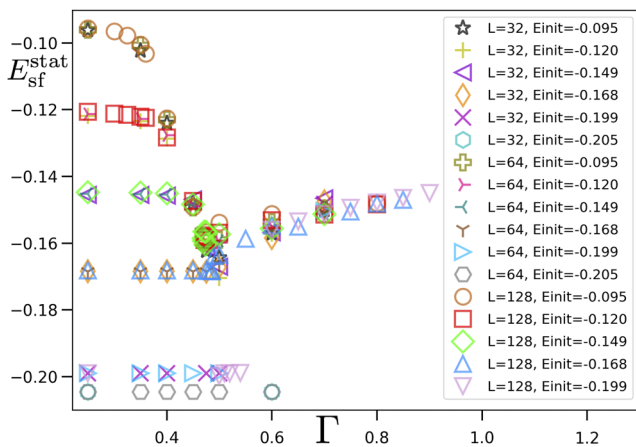


FIG. 9. E_{sf}^{stat} vs Γ for all system sizes and initial conditions E_{init} as indicated in the figure.

with $K > 0$ being a constant independent of the system size. A simple guess, by taking arguments from Ref. 37, is $x \approx 1/2$, and this yields our empirically observed $\alpha \approx 1/2$ while identifying Γ_0 with γ_y (Fig. 3)

Now two scenarios are possible: (i) if $\gamma_y = \Gamma^*$, the transition is of second order in nature as the fraction of the liquid material vanishes at the transition. (ii) If $\gamma_y < \Gamma^*$, the transition is of first order in nature as the fraction of the liquid material (shear band) is finite at the transition Γ^* . We can argue that the second scenario is correct. Indeed, γ_y is the elastic strain beyond which a liquid-state material (of E_{liq}) melts and its stress-strain curve bends.¹ By our model construction, we have $|E_{liq}| \propto \gamma_y^2$. On the other hand, for a critical marginal solid, we have $|E^*| \propto \Gamma^{*2}$ by its definition. Thus, we have $\Gamma^* \propto \sqrt{|E^*|} > \sqrt{|E_{liq}|} \propto \gamma_y$.

Combining the above arguments and our empirical data analysis, we can conclude for the stress-free energy of poorly annealed samples that $E_{sf}^{stat}(\Gamma^{*-}) = E^* < E^* + K(E_{liq} - E^*)(\Gamma^* - \gamma_y)^\alpha = E_{sf}^{stat}(\Gamma^{*+})$, i.e., a discontinuity across Γ^* with the predicted jump (~ 0.0045) appearing consistent with the fluctuation amplitude in the inset of Fig. 1(b).

APPENDIX E: DURATION OF THE OSCILLATORY TRANSIENT REGIME

The number of cycles needed to reach the stationary state is an observable that is expected to diverge at the transition, as seen equally in molecular dynamics of sheared amorphous solids^{14,15} and in models of sheared vortices in disordered media.^{39,40} We show in Fig. 10 the number n_T of oscillation cycles needed to reach the stationary state in our system for $\Gamma < \Gamma_c$ and $E_{init} > E^*$. n_T is easily measured in such situations since the stationary state is unambiguously identified once a perfect periodic loop of stress/energy (e.g., the blue curves in Fig. 8) is established. Instead of a power-law divergence,^{14,15} we observe rather $n_T \propto \log\left(\frac{1}{\Gamma_c - \Gamma}\right)$. The stationary state of well annealed systems $E_{init} < E^*$ oscillated at $\Gamma < \Gamma_c$ (E_{init}) is strongly reminiscent of its initial condition, as mentioned in the main text, and thus reached almost immediately. Only at Γ very

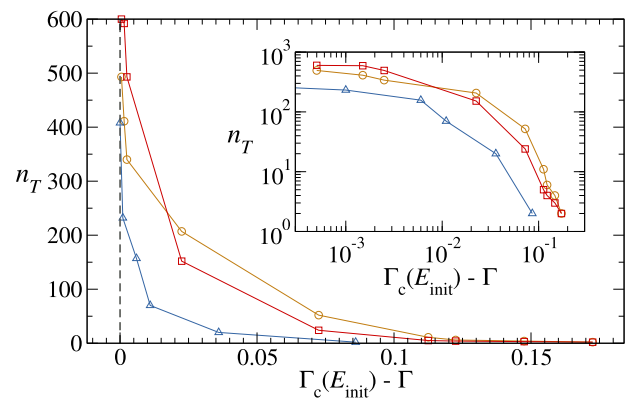


FIG. 10. Number of cycles needed to reach the steady state as a function of the distance to the critical amplitude for different initial annealing levels E_{init} .

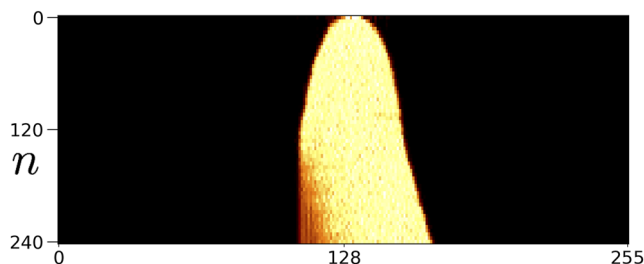


FIG. 11. The energy profile across a section perpendicular to the shear band evolving as a function of the number n of oscillation cycles. The light color region represents the position of the shear band with a higher energy. The amplitude of the oscillation is $\Gamma = 0.7$. The sample, of linear size $L = 256$, has initially been prepared at $E_{\text{init}} \approx -0.199$, i.e., in a very well annealed state.

close to Γ_c , a slight increase in n_T is observed due to the increased local adjustment, the nature of which is an open question. Above Γ_c , when Γ is approaching Γ_c , the system suffers a drastic dynamic slowing down that makes an accurate measurement of n_T more difficult. A more careful assessment of the specific law displayed by our model for the divergence of n_T at Γ_c is left for future investigation.

APPENDIX F: SHEAR-BAND EMERGENCE IN WELL ANNEALED SAMPLES

In Fig. 11, we show a color-map image similar to Fig. 4 of the main text. It depicts the energy profile evolution as a function of the number of oscillation cycles n in the first stages of the transient dynamics of an initially well annealed sample (here a sample of system size $L = 256$ for a better visualization). The inverted parabolic-like shape observed as n increases illustrates the band coarsening. In fact, the bandwidth growth law is rather $w \sim n^{1/3}$. At about $n \sim 120$ steps, the band has reached a stable width and starts moving ballistically to the right, leaving behind a marginal solid.

REFERENCES

- ¹D. Bonn, M. M. Denn, L. Berthier, T. Divoux, and S. Manneville, "Yield stress materials in soft condensed matter," *Rev. Mod. Phys.* **89**, 035005 (2017).
- ²A. Nicolas, E. E. Ferrero, K. Martens, and J.-L. Barrat, "Deformation and flow of amorphous solids: Insights from elastoplastic models," *Rev. Mod. Phys.* **90**, 045006 (2018).
- ³Y. Shi and M. L. Falk, "Atomic-scale simulations of strain localization in three-dimensional model amorphous solids," *Phys. Rev. B* **73**, 214201 (2006).
- ⁴M. Ozawa, L. Berthier, G. Biroli, A. Rosso, and G. Tarjus, "Random critical point separates brittle and ductile yielding transitions in amorphous materials," *Proc. Natl. Acad. Sci.* **115**, 6656–6661 (2018).
- ⁵M. Popović, T. W. J. de Geus, and M. Wyart, "Elastoplastic description of sudden failure in athermal amorphous materials during quasistatic loading," *Phys. Rev. E* **98**, 040901 (2018).
- ⁶H. J. Barlow, J. O. Cochran, and S. M. Fielding, "Ductile and brittle yielding in thermal and athermal amorphous materials," *Phys. Rev. Lett.* **125**, 168003 (2020).
- ⁷M. Ozawa, L. Berthier, G. Biroli, and G. Tarjus, "Rare events and disorder control the brittle yielding of amorphous solids," [arXiv:2102.05846](https://arxiv.org/abs/2102.05846) (2021).
- ⁸D. Richard, C. Rainone, and E. Lerner, "Finite-size study of the athermal quasistatic yielding transition in structural glasses," *J. Chem. Phys.* **155**, 056101 (2021).
- ⁹S. M. Fielding, "Yielding, shear banding and brittle failure of amorphous materials," [arXiv:2103.06782](https://arxiv.org/abs/2103.06782) (2021).
- ¹⁰D. Fiocco, G. Foffi, and S. Sastry, "Encoding of memory in sheared amorphous solids," *Phys. Rev. Lett.* **112**, 025702 (2014).
- ¹¹P. Leishangthem, A. D. S. Parmar, and S. Sastry, "The yielding transition in amorphous solids under oscillatory shear deformation," *Nat. Commun.* **8**, 14653 (2017).
- ¹²P. Das, A. D. S. Parmar, and S. Sastry, "Annealing glasses by cyclic shear deformation," [arXiv:1805.12476](https://arxiv.org/abs/1805.12476) (2020).
- ¹³D. Hexner, A. J. Liu, and S. R. Nagel, "Periodic training of creeping solids," *Proc. Natl. Acad. Sci.* **117**, 31690–31695 (2020).
- ¹⁴S. Sastry, "Models for the yielding behavior of amorphous solids," *Phys. Rev. Lett.* **126**, 255501 (2021).
- ¹⁵K. Khirallah, B. Tyukodi, D. Vandembroucq, and C. E. Maloney, "Yielding in an integer automaton model for amorphous solids under cyclic shear," *Phys. Rev. Lett.* **126**, 218005 (2021).
- ¹⁶W.-T. Yeh, M. Ozawa, K. Miyazaki, T. Kawasaki, and L. Berthier, "Glass stability changes the nature of yielding under oscillatory shear," *Phys. Rev. Lett.* **124**, 225502 (2020).
- ¹⁷T. Kawasaki and L. Berthier, "Macroscopic yielding in jammed solids is accompanied by a nonequilibrium first-order transition in particle trajectories," *Phys. Rev. E* **94**, 022615 (2016).
- ¹⁸I. Regev, T. Lookman, and C. Reichhardt, "Onset of irreversibility and chaos in amorphous solids under periodic shear," *Phys. Rev. E* **88**, 062401 (2013).
- ¹⁹I. Regev, J. Weber, C. Reichhardt, K. A. Dahmen, and T. Lookman, "Reversibility and criticality in amorphous solids," *Nat. Commun.* **6**, 8805 (2015).
- ²⁰D. Fiocco, G. Foffi, and S. Sastry, "Oscillatory athermal quasistatic deformation of a model glass," *Phys. Rev. E* **88**, 020301 (2013).
- ²¹N. V. Priezjev, "Reversible plastic events during oscillatory deformation of amorphous solids," *Phys. Rev. E* **93**, 013001 (2016).
- ²²N. V. Priezjev, "Collective nonaffine displacements in amorphous materials during large-amplitude oscillatory shear," *Phys. Rev. E* **95**, 023002 (2017).
- ²³I. Regev and T. Lookman, "The irreversibility transition in amorphous solids under periodic shear," in *Avalanches in Functional Materials and Geophysics* (Springer, 2017), pp. 227–259.
- ²⁴I. Regev and T. Lookman, "Critical diffusivity in the reversibility-irreversibility transition of amorphous solids under oscillatory shear," *J. Phys.: Condens. Matter* **31**, 045101 (2018).
- ²⁵M. Mungan, S. Sastry, K. Dahmen, and I. Regev, "Networks and hierarchies: How amorphous materials learn to remember," *Phys. Rev. Lett.* **123**, 178002 (2019).
- ²⁶H. Bhaumik, G. Foffi, and S. Sastry, "The role of annealing in determining the yielding behavior of glasses under cyclic shear deformation," *Proc. Natl. Acad. Sci.* **118**, e2100227118 (2021).
- ²⁷A. D. S. Parmar, S. Kumar, and S. Sastry, "Strain localization above the yielding point in cyclically deformed glasses," *Phys. Rev. X* **9**, 021018 (2019).
- ²⁸P. Das, H. A. Vinutha, and S. Sastry, "Unified phase diagram of reversible-irreversible, jamming, and yielding transitions in cyclically sheared soft-sphere packings," *Proc. Natl. Acad. Sci.* **117**, 10203–10209 (2020).
- ²⁹E. A. Jagla, "Strain localization driven by structural relaxation in sheared amorphous solids," *Phys. Rev. E* **76**, 046119 (2007).
- ³⁰I. Fernández Aguirre and E. A. Jagla, "Critical exponents of the yielding transition of amorphous solids," *Phys. Rev. E* **98**, 013002 (2018).
- ³¹E. E. Ferrero and E. A. Jagla, "Elastic interfaces on disordered substrates: From mean-field depinning to yielding," *Phys. Rev. Lett.* **123**, 218002 (2019).
- ³²E. A. Jagla, "Tensorial description of the plasticity of amorphous composites," *Phys. Rev. E* **101**, 043004 (2020).
- ³³E. E. Ferrero and E. A. Jagla, "Properties of the density of shear transformations in driven amorphous solids," *J. Phys.: Condens. Matter* **33**, 124001 (2021).
- ³⁴J. Lin, E. Lerner, A. Rosso, and M. Wyart, "Scaling description of the yielding transition in soft amorphous solids at zero temperature," *Proc. Natl. Acad. Sci.* **111**, 14382–14387 (2014).

- ³⁵J. D. Eshelby, "The determination of the elastic field of an ellipsoidal inclusion, and related problems," *Proc. R. Soc. A* **241**, 376–396 (1957).
- ³⁶M. L. Manning, J. S. Langer, and J. M. Carlson, "Strain localization in a shear transformation zone model for amorphous solids," *Phys. Rev. E* **76**, 056106 (2007).
- ³⁷E. A. Jagla, "Shear band dynamics from a mesoscopic modeling of plasticity," *J. Stat. Mech.: Theory Exp.* **2010**, P12025.
- ³⁸N. Mangan, C. Reichhardt, and C. J. O. Reichhardt, "Reversible to irreversible flow transition in periodically driven vortices," *Phys. Rev. Lett.* **100**, 187002 (2008).
- ³⁹S. Okuma, Y. Tsugawa, and A. Motohashi, "Transition from reversible to irreversible flow: Absorbing and depinning transitions in a sheared-vortex system," *Phys. Rev. B* **83**, 012503 (2011).
- ⁴⁰B. L. Brown, C. Reichhardt, and C. J. O. Reichhardt, "Reversible to irreversible transitions in periodically driven skyrmion systems," *New J. Phys.* **21**, 013001 (2019).
- ⁴¹S. Maegochi, K. Ienaga, and S. Okuma, "Critical behavior of density-driven and shear-driven reversible–irreversible transitions in cyclically sheared vortices," *Sci. Rep.* **11**, 19280 (2021).
- ⁴²X. Cao, A. Nicolas, D. Trimcev, and A. Rosso, "Soft modes and strain redistribution in continuous models of amorphous plasticity: The Eshelby paradigm, and beyond?," *Soft Matter* **14**, 3640–3651 (2018).
- ⁴³D. Denisov, M. Dang, B. Struth *et al.*, "Sharp symmetry-change marks the mechanical failure transition of glasses," *Sci. Rep.* **5**, 14359 (2015), <https://www.nature.com/articles/srep14359>.